Bulletin of the Geological Survey of Japan, vol. 49 (11), p. 551-569, 1998

Nanometer-scale structures in a Mn-Mg-Fe Amphibole from Vittinki Group, Western Finland

Franco MANCINI*, Katsumi MARUMO*, Reijo ALVIOLA**, Norihiko KOHYAMA*** and Brian MARSHALL†

Franco MANCINI, Katsumi MARUMO, Reijo ALVIOLA, Norihiko KOHYAMA and Brian MARSHALL (1998) Nanometer-scale structures in a Mn-Mg-Fe Amphibole from Vittinki Group, Western Finland. *Bull. Geol. Surv. Japan*, vol. 49 (11), p. 551-569, 14 figs., 4 tables.

Abstract: Samples of Mn-Mg-Fe amphibole from regionally metamorphosed (T=650-700°C, P=4-6 kbars) quartz-Mn-Mg-Fe amphibole veins intercalated with Mn-rich gneiss in the Vittinki Group, western Finland, have been studied by analytical transmission electron microscopy (ATEM). The results show that the Mn-Mg-Fe amphibole is exsolved on a submicroscopic scale and contains abundant lamellae of Mn-rich actinolitic amphibole, consistent with unmixing from an homogeneous amphibole upon cooling. The lamellae are coherently intergrown with the host and occur in two orientations, nearly parallel to ($\bar{1}01$) and (100) planes of the host, consistent with previously reported lamellar orientation for monoclinic amphiboles. Their exact orientation varies 11° for the "100" set and 6° for the "$\bar{1}01$" set, indicating exsolution over a large temperature range. Furthermore, the "100" lamellae have widths between 70 and 150 nm, whereas the "$\bar{1}01$" lamellae show a larger range, 150-700 nm, which do not correlate with the orientation and that presumably reflect local variations in the diffusivity of chemical elements.

High resolution TEM images of the Mn-Mg-Fe amphibole show rare 'faults' which consist of triple-chain lamellae (5-10 nm, at most, in the b-direction), in a predominantly ordered double-chain host. In contrast, many Mn-Mg-Fe amphibole grains show topotactic replacement to talc as is evidenced by chemical compositions intermediate between amphibole and talc.

1. Introduction

Metamorphic amphiboles can contain micrometer- to nanometer-scale intergrowths which are too fine-grained to be observed by a conventional petrographic microscope but that can be characterized in detail by a transmission electron microscope (TEM) equipped with an analytical system (AEM). In particular, exsolution or unmixing upon cooling from an homogeneous primary phase originate micrometer-scale exsolution lamellae whose orientation and composition can be used to elucidate the thermal history of metamorphic rocks (e.g. Klein *et al.*, 1996, 1997). Furthermore, solid state replacement reactions produce nanometer-scale lamellae of triple, quadruple, septuple chains, etc., parallel to the amphibole double chain, that have recently received much attention as petrogenetic indicators of metasomatism under crustal conditions (Schumaker and Czank, 1987; Akai, 1988; Akai *et al.*, 1997). Triple-chain lamellae have also been described in natural and synthetic Mn-Mg-Fe amphiboles (e.g. Akai, 1982; Maresch and Czank, 1987), and were identified by high resolution electron imaging (HREM) techniques that allow the observation of minerals at or close to the atomic scale.

In this article we report the results of a TEM-AEM study of a Mn-Mg-Fe amphibole from the Svecofennian Vittinki Group, western Finland. Preliminary investigations (R. Alviola, unpubl.) identified lamellar intergrowths and showed that some of the chemical formulae determined from electron microprobe analysis have too high tetrahedral to octahedral cation ratios.

2. Geologic setting and sample location

The Vittinki Group (VTG), which was sampled for this study, lies within the 1.97-1.88 Ga Svecofennian domain in southwest Finland (Fig. 1). It is part of a tract of supracrustal gneiss, representing the northwestern continuation of the Tampere Schist Belt (TSB), that hosts well-preserved volcano-sedimentary sequences (e.g. Kähkonen, 1994). The Svecofennian

* Mineral and Fuel Resources Department, GSJ
** Geological Survey of Finland, P.O.Box 96, FIN-02151 ESPOO, Finland
*** National Institute of Industrial Health, 21-1 Nagao 6-chome, Tama-ku Kawasaki 214
† Department of Applied Geology, University of Technology, Sydney, P.O.Box 123, Sydney, Australia

Keywords: Precambrian, Finland, metamorphism, manganese, minerals, chain silicates, transmission electron microscope, twinning.

(a)

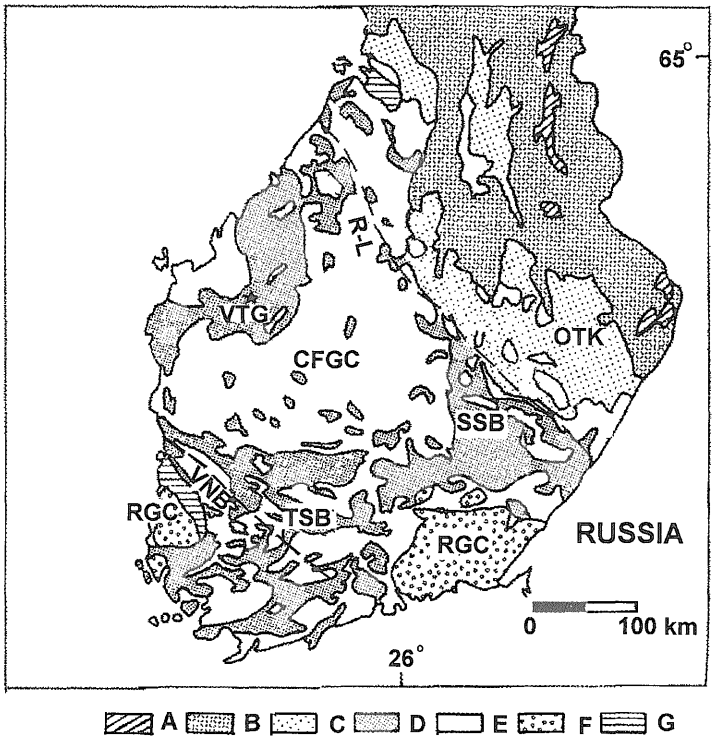

(b)

Fig. 1 a: main geologic units of the Baltic Shield and location of the early Proterozoic island arcs (stippled areas) (modified after Ekdahl, 1993). b: Schematic geologic map of central and south Finland (after A. Simonen). The star indicates the location of the sampled Vittinki Group (VTG). Legend: A=Archean greenstone belt; B=Archean granitoids; C=Karelian supracrustal rocks; D=Svecofennian supracrustal rocks; E=Svecokarelian granitoids; F=Rapakivi granites; G=Jotnian sediments, (see text for abbreviations).

domain has been interpreted as a paleosuture (e.g. Hietanen, 1974; Papunen and Gorbunov, 1985; Huhma, 1986; Gaál and Gorbatchev, 1987; Gaál, 1990; BABEL, 1990; Ruotoistenmäki, 1996) which, by analogy with present-day collision zones in the western Pacific, involves subduction of the oceanic Svecofennian plate beneath the Karelian continent and the concurrent development of complex island arc systems (Fig. 1a). The latter include the Pyhäsalmi island arc (PIA) on the continent margin, similar to the modern Japan arc, and the oceanic Tampere-Vasa (TIA) and Orijärvi (OA) island arcs (e.g. Gaál and Gorbatchev, 1987; Gaál, 1990). In the Outokumpu (OTK) district, the 1.97 Ga serpentinites and black schist with Cu-Zn-Ni-Co-Cr-Au mineralisation have been interpreted as ophiolites formed during rifting and sea floor spreading in a back-arc basin located on the western margin of the Karelian craton (e.g. Gaál, 1990; Ekdahl, 1993). In the Tampere and Savo Schist Belts (TSB and SSB respectively), the amphibolites, micaschists and gneisses, together with their tuffaceous intercalations, have been interpreted as volcano-sedimentary deposits formed in back-arc basins (Kähkonen, 1994; Lahtinen, 1996), while the arc and back-arc magmatism are represented by the granites, granodiorites and gabbros of the central Finland granitic complex (CFGC) (e.g. Huhma, 1986; Ekdahl, 1993). In the NNW-SSE trending Raahe-Ladoga zone (R-L) and Vammala Nickel Belt (VNB), the ultramafic-mafic intrusions and associated Ni-Cu deposits supposedly represent tholeiitic magmas that were generated by partial melting of subducted oceanic crust (e.g. Papunen and Gorbunov, 1985; Mäkinen, 1987; Peltonen, 1995); on the other hand, by analogy with island arc-hosted Kuroko-type deposits, the Zn-Cu-Pb massive sulfides, with well-preserved sedimentary structures, are interpreted as the products of a submarine hydrothermal system (Gaál, 1990; Ekdahl, 1993).

The main closing stage of the Svecofennian orogeny occurred 1.90–1.86 Ga ago (Fig. 2-Ruotoistenmäki, 1996), when the central Finland island arcs and back arc basins were thrust against the Karelian continent. The N-NE thrusting formed recumbent folds (e.g. Simonen, 1980) and was accompanied by granulite facies metamorphism at temperatures of 800–880°C and pressures of 5–6 kbars in the northern PIA arc (Korsman *et al.*, 1984; Korsman, 1988) and temperatures from 600–650°C at 7–8 kbars to 700–720°C at 4–6 kbars in the southern Tampere-Vasa (TIA) arc (e.g. Kilpeläinen and Rastas, 1992; Kilpeläinen *et al.*, 1994). The counterclockwise rotation of the Svecofennian thrusting from NE to N (Fig. 2) explains: (a) the rotation of the TIA arc around the PIA arc (e.g. Ekdahl, 1993; Ruotoistenmäki, 1996); and (b) the oblique collision which formed the NW-trending deep-seated faults and shear zones that possibly controlled the emplacement of Ni-bearing ultramafic-mafic intrusions in the R-L zone and VNB belt (e.g. Gaál, 1990). Field and petrologic data indicate that after the peak metamorphism, the Svecofennides in south-western Finland were rapidly exhumated which have resulted in a nearly isothermal decompression, possibly to pressure of 1–2 kbars (e.g. Kilpeläinen and Rastas, 1992; Mancini *et al.*, 1996). The peak metamorphic upper amphibolite-lower granulite facies mineral assemblages were later overprinted by the hornblende-hornfels assemblages during the M2 retrograde metamorphism at temperature of 530–560°C (e.g. Kilpeläinen and Rastas, 1992).

The Vittinki Group is known for its manganese-bearing horizons. The bedrock is poorly exposed in the area but outcrops of volcanics, chert, and graphite-bearing gneisses with Fe-Mn mineralization have been reported (Saxén, 1925). The ore occurs as concordant layered bodies within biotite-plagioclase gneiss, in turn hosted by quartzites (Törnroos, 1982). The Mn-rich lenses and pods are mainly rhodonite/pyroxmangite rocks with minor amounts of other Mn-minerals (i.e. pyroxene, amphiboles, quartz and Mn-oxides and Mn-sulfides, e.g. alabandite) (Törnroos, 1982). These manganiferous iron formations with abundant silicate facies (i.e. manganiferous cherts) are relatively abundant in the Svecofennides near the boundary of the Archaean craton but less common in the southern part (e.g. Ekdahl, 1993). They have been interpreted as syngenetic deposits of iron, manganese, silica and phosphorous formed at shallow depth in a

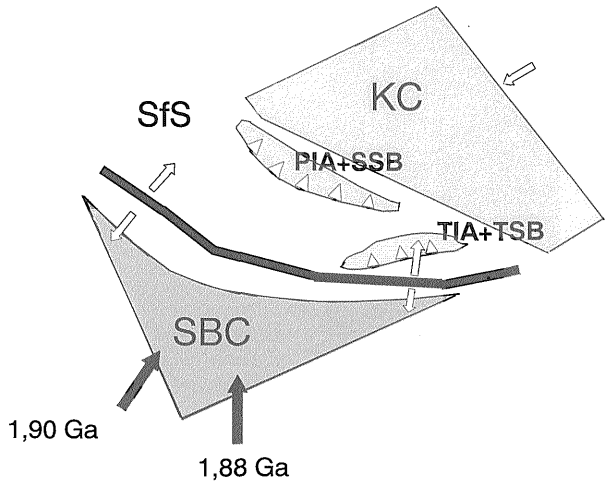

Fig. 2 Plan view of the evolution of the Svecofennian island arc systems at the onset of the closing stage, 1.90–1.88 Ga ago, according to T. Ruotoistenmäki (1996). The black arrows indicate the directions of thrusting. Abbreviations: KC=Karelian continent; SBC=Svecobaltian continent; SfS=Svecofennian sea; PIA+SSB=Pyhäsalmi island arc and *Savo Schist Belt;* TIA+TSB=Tampere-Vasa island arc and *Tampere Schist Belt.*

back-arc basin about 2.0–1.97 Ga ago (Ekdahl, 1993). It is noteworthy that the quartz-rocks have been interpreted as recrystallized cherts rather than primary clastic sediments (e.g. Tuukki, 1984).

3. Sample description

In the Mn-horizons at Vittinki, Mn-Mg-Fe amphibole occurs as porphyroblasts, small Mn-Mg-Fe amphibole-kanoite/johannsenite patches, or quartz-Mn-Mg-Fe amphibole veins which are less than 10 cm wide. The samples for this study are from a quartz-Mn-Mg-Fe amphibole vein (Fig. 3) in which porphyroblastic and nematoblastic Mn-Mg-Fe amphiboles coexist with minor Ca-Mg-Mn pyroxenes and Mn-rich tremolitic amphibole, and are dispersed in a quartz matrix. Mn-oxides form boudin-shaped clusters within the quartz-Mn-Mg-Fe amphibole matrix and consist mainly of fine grained cryptomelane/psilomelane (MnO_2), with a typical low hardness. The silicate minerals have a slight preferred orientation and thereby define a weak schistosity. Their straight common grain boundaries are indicative of an equilibrium assemblage. Colorless amphiboles and pyroxene, which could not easily be distinguished in thin section, were identified on the basis of their compositions (Table 1). The Mn-Mg-Fe amphiboles have Mn-content ranging 1.26–1.65 apfu and they are manganocummingtonite of Leake *et al.* (1997); they differ significantly with respect to the $Mg/Mg+Fe^{2+}$ ratio, between 0.56 and 0.92, that presumably reflect variation in the $Mg/Mg+Fe^{2+}$ ratio of the host rock (in prep.) The $K_D[(Mg/Mn)_{Ca-Mg-Mn\ pyroxene}/(Mg/Mn)_{Mn-Mg-Fe\ amphibole}]$ varies between 0.72 and 1.40. Synkinematic growth is supported by the (100) deformational twinning of Mn-Mg-Fe amphibole, while retrogressive deformation is evidenced by the grain-size reduction of quartz. The Mn-Mg-Fe amphibole crystals host small ($\leq 1\mu$m) quartz inclusions and thin lamellae, that have an orientation consistent with that for "$\bar{1}01$" exsolution lamellae in clinoamphiboles. Assemblages similar to those described occur in other metamorphosed manganese-bearing sediments at upper amphibolite-lower granulite facies (T=650–700°C at P=4–6 kbars-Kobayashi, 1977; Dasgupta *et al.*, 1988). At Vittinki, the same peak metamorphic conditions are consistent with the extensive development of migmatites in the adjacent garnet+biotite+sillimanite+cordierite-bearing micagneisses.

4. Analytical methods

Two sets of samples were prepared for transmission electron microscopy (TEM). The first set was prepared by ion milling. A disc, 3 mm in diameter, was removed from a thin section using an ultrasonic cutter

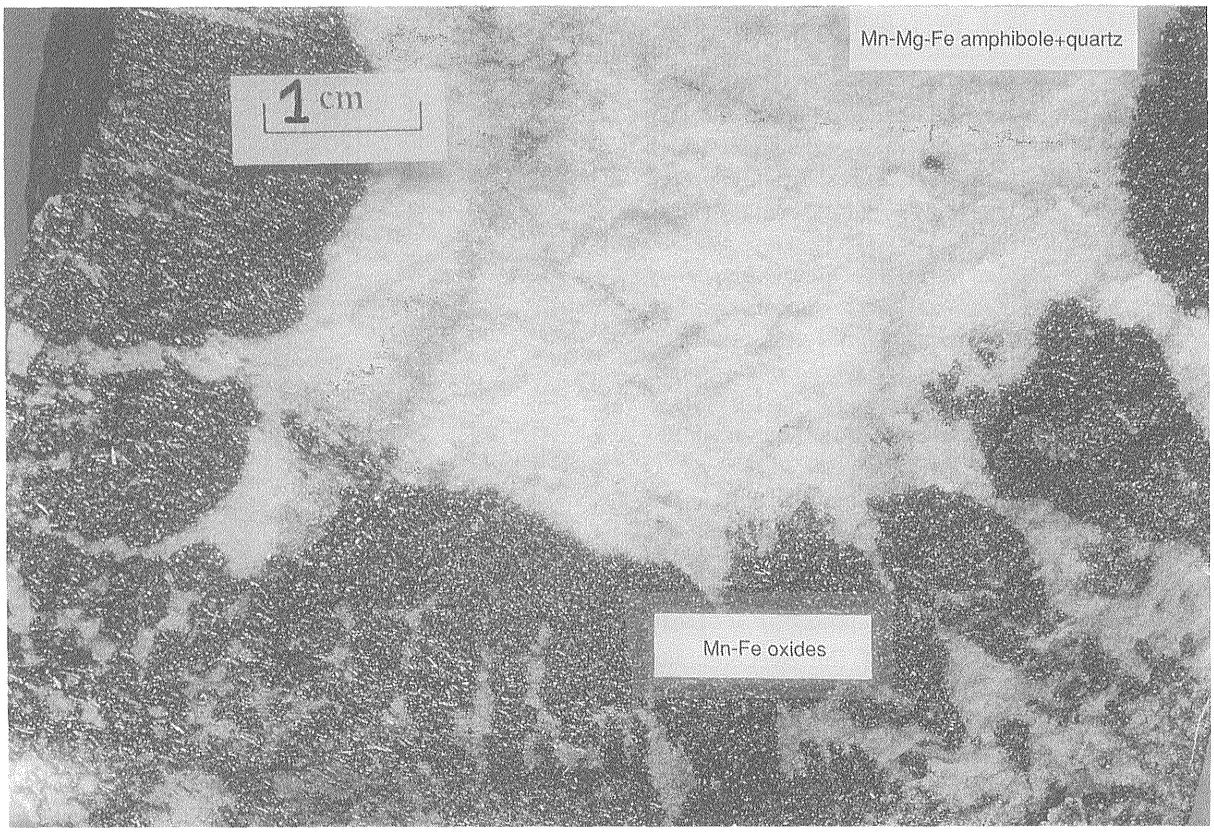

Fig. 3 Hand sample of a quartz-Mn-Mg-Fe amphibole vein from the Vittinki Group, Finland.

Table 1 EPMA analysis and chemical formulae of Mn-Mg-Fe amphiboles (MnMgFe-amp), Mn-rich tremolitic amphibole (tr) and Ca-Mg-Mn pyroxene (CaMgMn px) in the quartz-Mn-Mg-Fe amphibole vein, Vittinki Group, Finland.

	MnMg Fe-amp	MnMg Fe-amp	MnMg Fe-amp	tr	tr	CaMgMn px	CaMgMn px
SiO_2	57.00	54.70	51.60	54.10	55.41	51.99	52.00
TiO_2	0.00	0.00	0.00	0.00	0.03	0.03	0.03
Al_2O_3	0.00	0.00	0.00	0.00	0.19	0.01	0.01
Cr_2O_3	0.00	0.00	0.00	0.00	0.00	0.04	0.02
FeO	3.60	12.00	18.00	6.00	2.02	1.69	1.69
MnO	12.10	10.20	12.60	6.80	9.41	9.78	9.79
MgO	24.30	19.20	13.00	18.60	21.07	13.95	13.61
CaO	1.20	0.60	1.00	9.00	8.19	21.45	21.38
Na_2O	0.00	0.00	0.00	0.00	0.24	0.13	0.13
K_2O	0.00	0.00	0.00	0.00	0.12	0.01	0.00
F	1.60	1.10	0.10	0.70	0.87	0.00	0.00
H_2O	0.00	n.d.	n.d.	n.d.	n.d.	–	–
total	99.80	97.80	96.30	95.20	97.55	99.08	98.66
	23 O	*23 O*	*23 O*	*23 O*	*23 O*	*6 O*	*6 O*
Si	7.95	7.99	7.94	7.96	7.89	1.98	1.98
Al	0.00	0.00	0.00	0.00	0.03	0.00	0.00
Ti	0.00	0.00	0.00	0.00	0.00	0.00	0.00
Fe^{2+}	0.42	1.46	2.31	0.74	0.24	0.05	0.05
Mg	5.05	4.18	2.98	4.08	4.47	0.79	0.79
Mn	1.43	1.26	1.64	0.84	1.13	0.31	0.31
Ca	0.18	0.09	0.16	1.42	1.25	0.87	0.87
Na	0.00	0.00	0.00	0.00	0.06	0.01	0.01
K	0.00	0.00	0.00	0.00	0.02	0.00	0.00
Mg/Mn	3.53	3.31	1.81	4.85	3.95	2.54	2.54

[1] Analyst R. Alviola, Geological Survey of Finland

and dimpled to 20-30 microns. It was then glued to a single-aperture copper grid. The beam milling was performed at angles varying between 18° and 8° using 4 keV argon particles. The second set consisted of a small quantity of powdered material crushed and dispersed in water. The resulting suspension was deposited on a carbon holey film supported on a standard mesh grid, 3 mm in diameter.

Electron microscopy was performed with a Philips CM12 transmission electron microscope operated at 100 keV. A Super Twin (ST) objective lens (spherical aberration coefficient Cs=1.2 mm, chromatic aberration Cc=1.2 mm) was used. Energy dispersive X-ray spectra (EDS) were obtained with an EDAX SiLi ultra-thin window detector using a 100-second acquisition time. During analysis, the specimen was tilted about 7° towards the detector, thus yielding a total take-off angle of 23°. The compositions were calculated from the intensities using the method of Cliff and Lorimer (1972). The method states that, for a very thin specimen (<100-200nm), the effects of X-ray absorption and fluorescence can be neglected so that the concentration ratios for any two elements (C_i/C_j) are related to their X-ray intensity ratios (I_i/I_j) by the equation $I_i/I_j = kC_i/C_j$. Relative to Si, k-values were calculated for each element of interest using standards: phlogopite for Mg, K and Al, johannsenite for Mn and Ca, enstatite for Mg and Fe, and kaolinite for Al. Compositions of the standards were accurately determined by a JEOL microprobe, equipped with a WDS detector, at a 200 sec^{-1} counting rate (Appendix

Table 2 Experimental K-values (molecular ratio) of each element respect to Si.

	mean
Mg	1.34(1)[1]-1.47(1)[2]
Al	1.12(0.4)*
Si	1.00
Ca	0.90(6)-0.81(5)*
K	0.95(5)
Fe	0.72(0.8)
Mn	0.85(4)-0.83(5)*

[1,2] calculated with phlogopite and enstatite, respectively.
* calculated from powdered standard.
N.B. the standard deviations (in parenthesis) refer to the last digit.

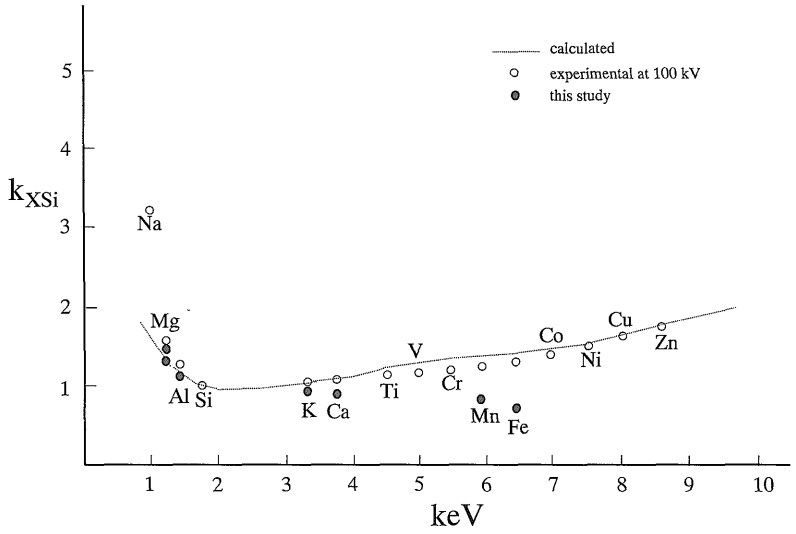

Fig. 4 Experimental $k_{x,si}$ values at 100 keV plotted against the characteristic energy of the elements. Note the shift to lower values for the $k_{x,si}$ in this study compared with the experimental values of Cliff and Lorimer (1972) and the *ab initio* calculated values of Goldstein *et al.*, (1977). Note the large difference between $k_{x,si}$ for magnesium calculated with the enstatite standard, 1.47, and with the phlogopite standard, 1.34, (points 1 and 2 respectively).

1). The expression, $k_{x,Si}=M_{Si}/M_X \cdot I_X/I_{Si}$ (where M_X/M_{Si} is the mole ratio of the analyzed element relative to Si and I_X/I_{Si} the intensity ratio), was used because it provides a direct measure of the relative number of atoms in the chemical formula of the analyzed mineral. The intensity ratio (I_X/I_{Si} in the expression for $k_{x,si}$) was calculated by least-squares analysis of the plot of I_X versus I_{Si} (Appendix 2).

The k-values determined (Table 2) are plotted against the characteristic energy of each element in Fig. 4. Compared with the experimental k-values of Cliff and Lorimer (1975) and those calculated by Goldstein *et al.* (1977), our values, especially for the heavy elements, are rather low (<1.0). We ascribe this to the improved efficiency of X-ray detection.

High resolution TEM (HRTEM) was performed with the Philips CM12 at GSJ and also with the Hitachi 8000 TEM at 200 keV at the National Institute of Industrial Health (NIIH, Tokyo). An intermediate diameter objective aperture was used.

For accurate measurement of the lattice plane spacing, a calibration of the magnification was carried out using a grid with graphitised carbon black as standard.

5. Results

5.1 Exsolution lamellae

5.1.1 Orientation aspects

Two sets of exsolution lamellae in the Mn-Mg-Fe amphibole were observed, "$\bar{1}01$" and "100" (Fig. 5a,b), corresponding to the two most common lamellar orientations in clinoamphiboles. Chemical analysis confirmed that they are Mn-rich actinolitic amphibole [mangano-ferro-actinolite and manganoan actinolite of Leake *et al.*, (1997)] (Table 3). The orientations and widths of the lamellae (Table 4) were accurately measured using an ion-milled specimen (VTN3A) cut nearly parallel to the a*-c* plane. The sample was mounted with the a*-axis parallel to the tilt axis of the sample holder so that the a*-c* section could be attained by slightly tilting the goniometer. The lamellae of the "$\bar{1}01$" set are wider and have widths of 150–700 nm, probably due to faster diffusion parallel to the double chain of the amphibole structure, and are commonly wedge-shaped; the "100" set is less common and have widths of 70–150 nm. The large differences in the widths, especially of the "$\bar{1}01$" lamellae (Fig. 5b), which are unrelated to orientation, were possibly controlled by local increases in the diffusivity of chemical elements (discussed below).

The HRTEM images (Fig. 6) show that the lattices of the host and lamellae are continuous across the lamellar interface and adjust by slight rotation of the lattice fringes. According to optimal phase boundary theory (OPB-theory; Bollman and Nissen, 1968), the lamellae are parallel to planes of best dimensional fit between the lattices of the host and exsolved phases; their exact orientation changes slightly with the temperature of exsolution. The Mn-Mg-Fe amphibole studied has a large range of lamellar orientations (Table 4), the angle between the "$\bar{1}01$" lamellae and the a-axis of the host amphibole varies in the range 20.7–26.1° and that between the "100" lamellae and the c-axis of the host amphibole ranges across 6.5–17.9°, which is therefore consistent with multigenerational

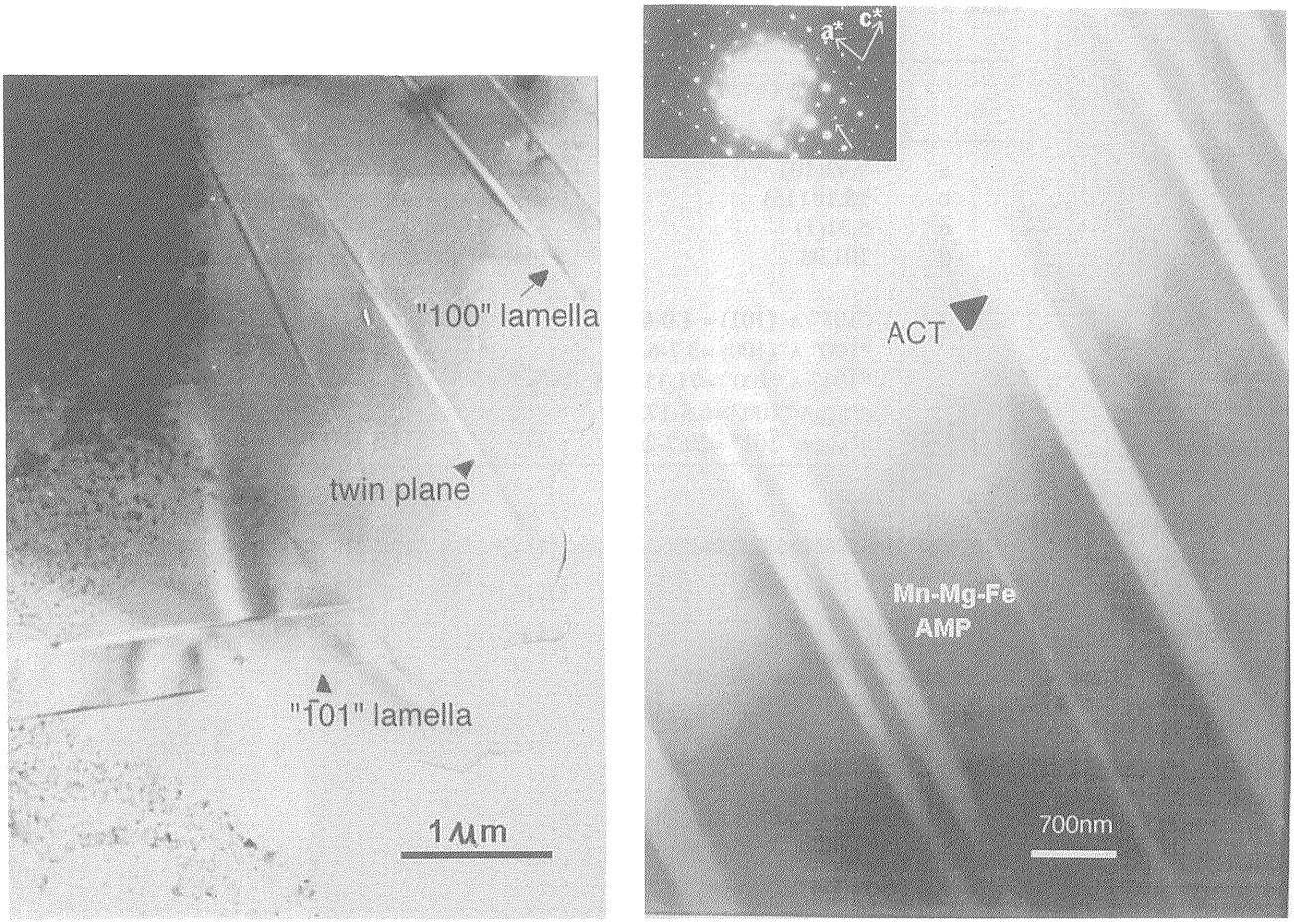

Fig. 5 a: TEM bright field image of the Mn-Mg-Fe amphibole host and the two sets of lamellae taken in a non zone axis orientation. The (100) twin plane is also shown. Note the spotted appearance of the argon-damaged areas (lower left corner). b: Low magnification TEM bright field image of the "$\bar{1}$01" lamellae showing a great range of lamellar widths. The inset is the a*-c* SAED pattern (selected area electron diffraction) of the same area. Note the splitting of the spots (arrowed) due to the slightly different lattice parameters of the host and exsolved phases.

Table 3 Selected AEM chemical formula of Mn-Mg-Fe amphibole (MnMgFe amp) host and Mn-rich actinolitic amphibole (act) lamellae.

	MnMgFe-amp	MnMgFe-amp	MnMgFe-amp	act	act	act
Si	8.00	8.00	8.00	8.00	8.00	8.00
Al	-	-	-	-	-	-
total	8.00	8.00	8.00	8.00	8.00	8.00
Mg	1.88	1.89	1.94	1.98	2.00	2.20
Fe^{2+}	2.50	2.59	2.73	2.15	2.17	1.73
Mn	0.62	0.53	0.34	1.17	1.12	0.79
total	5.00	5.00	5.00	5.00	5.00	4.72
Ca	0.35	0.42	0.44	2.00	1.97	2.00
Mn	1.65	1.58	1.56	-	0.03	-
total	2.00	2.00	2.00	2.00	2.00	2.00
$Mg/Mg+Fe^{2+}$	0.43	0.42	0.41	0.48	0.48	0.55
$Mn/Mn+ Fe^{2+}+Mg$	0.34	0.32	0.29	0.23	0.20	0.17

Table 4 Lattice parameters and orientation relationships of "$\bar{1}01$" and "100" exsolution lamellae in Mn-Mg-Fe amphibole.

	Mn-Mg-Fe amphibole host	"$\bar{1}01$" and "100" Mn-rich actinolitic lamellae
a	9.42(10)	9.67(15)
b	18.18 (15)	n.m.
c	5.31(1)	5.30(1)
β	101.98	104.9
	"$\bar{1}01$" ∧ ($\bar{1}01$) = 1.0-6.5	
	"100" ∧ (100) =3.7-6.1	
	"$\bar{1}01$" ∧ "100" =71.35-75.5	
	c^*_{host} ∧ "100" =6.5-17.9	
	a^*_{host} ∧ "$\bar{1}01$" =20.7-26.1	

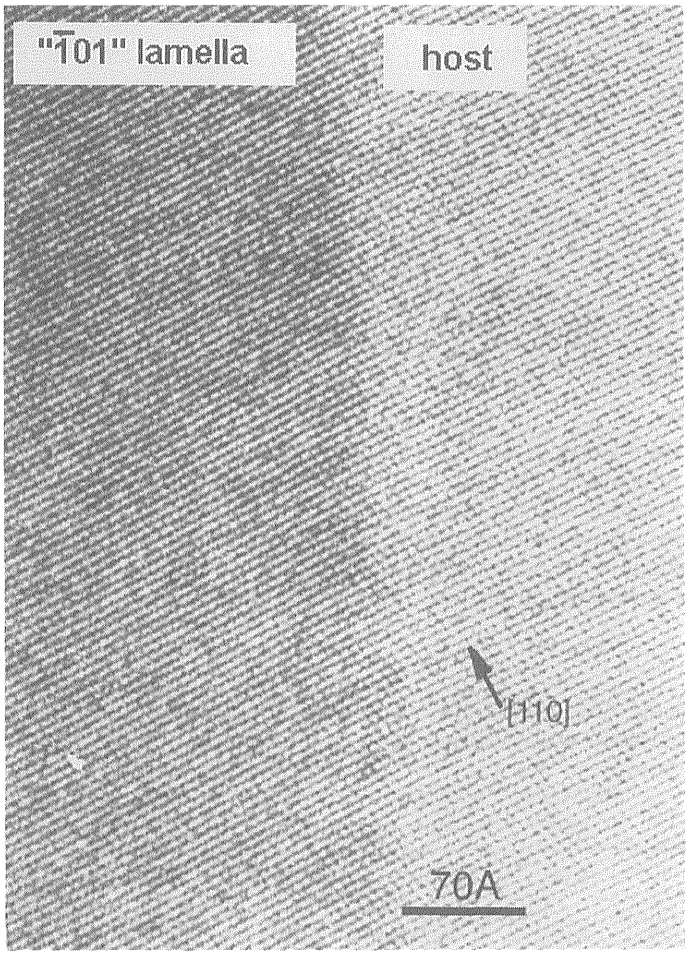

Fig. 6 A near [$\bar{1}20$] zone high resolution TEM image showing the (110) lattice fringes, d(110)= 0.84 nm, that are continuous across the lamellar boundaries, but with a slight rotation of 2.6° (best viewed with the direction of view nearly parallel to the page).

exsolution during the slow post-peak metamorphic cooling (e.g. Klein *et al.*, 1996).

5.1.2 Chemographic aspects

Representative compositions of the host and lamellae determined for ion-thinned samples are listed in Table 3. The chemical analyses were performed using a small (100-200 nm) beam spot size and a count rate of 100 s^{-1}. Because the "100" lamellae have narrow widths, of the order of the spatial resolution of the

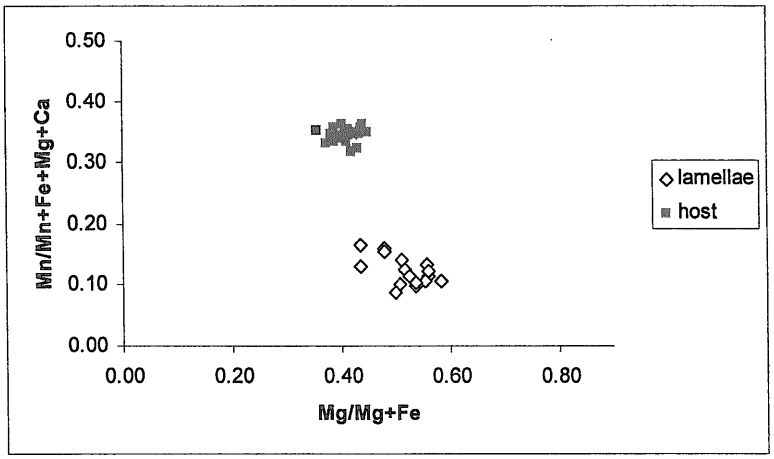

Fig. 7 A comparison of $Mg/Mg+Fe^{2+}$ and $Mn/Mn+Fe^{2+}+Mg+Ca$ ratios between Mn-Mg-Fe amphibole host and Mn-rich actinolitic amphibole lamellae. Note the miscibility gap which is defined in terms of the Mn → Ca substitution in the M4 site.

finest probe (~100 nm), only the large "$\bar{1}01$" lamellae were analyzed. The observation of lattice fringes in the analyzed areas substantiated the "thin-film" approximation, in that the maximum thickness for which microstructures in silicates can be observed at 100 keV is about 200 nm (Champness, 1977).

The structural formulae of the amphiboles (Table 3) were obtained by recalculating the AEM element ratios to 8-silica, as supported by the negligible Al content determined by electron microprobe analysis (EPMA) of amphiboles from Vittinki (Table 1). All Fe was considered bivalent, as suggested by the results of X-ray single crystal and Mössbauer spectroscopy, and the cations were assigned to the various crystallographic sites following the scheme of Robinson *et al.* (1982). The analysed host Mn-Mg-Fe amphiboles have $Mg/Mg+Fe^{2+}$ ratios less than 0.5 (0.38-0.43) (Table 3 and Fig. 7) and therefore they correspond to manganogrunerite of Leake *et al.* (1997). They also show distinctly higher $Mn/Mn+Fe^{2+}+Mg+Ca$ and lower $Mg/Mg+Fe^{2+}$ ratios than in Mn-rich actinolitic amphibole lamellae. These ratios define the compositional gap which largely occurs as a result of the $Mn(Fe^{2+})$→ Ca substitution in the M4 site of the amphibole structure. Compositional profiles between lamellae were obtained by step-analysis, with an averaging spacing of 200nm between analysed spots (Fig.

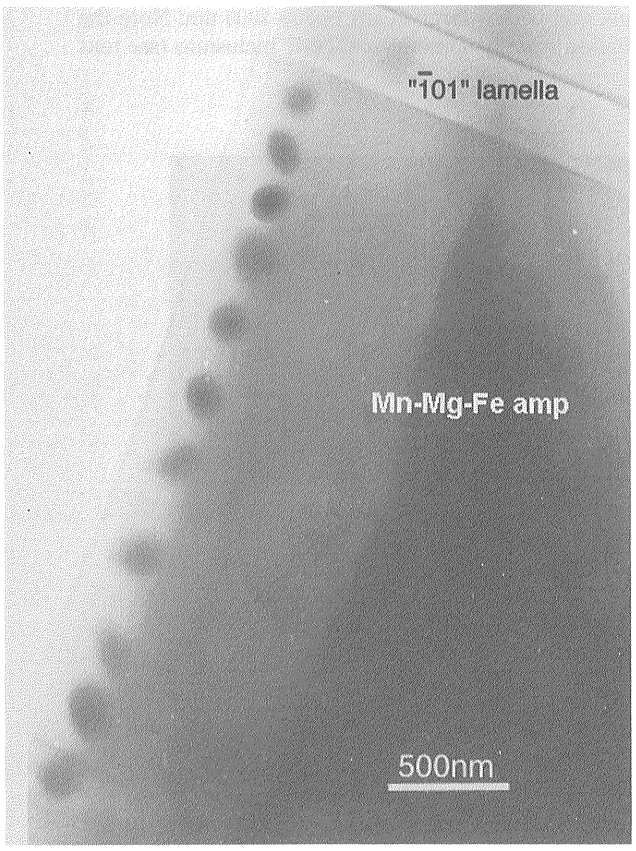

(a)

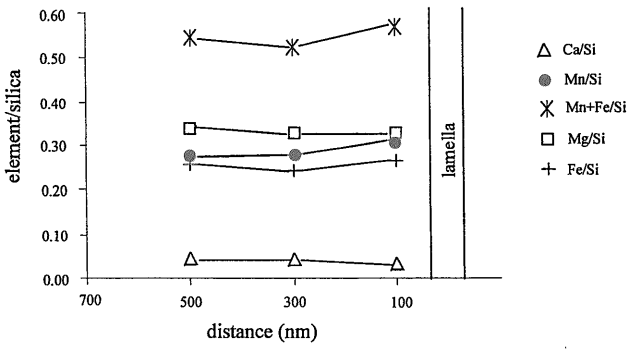

(b)

Fig. 8 a: TEM bright field image of the location of the step-scan profile adjacent to an actinolitic lamellae. b: Plot of distance vs. the relative concentration of Ca, Mn, Mg and Fe^{2+} in the Mn-Mg-Fe amphibole host.

8a,b). The results show an almost flat profile, consistent with an equilibrium condition. However, at a distance of about 100 nm from the lamellae, a Ca decrease and a Mn and Fe increase is ascribed to lamellar growth, during which Ca diffused towards, and Mn and Fe away from the lamellae, in agreement with previous studies (e.g. Klein *et al.*, 1997).

For powdered Mn-Mg-Fe amphibole samples free of lamellae, a larger spot size (800–2000 nm) was used; this improved the counting statistic but had the disadvantage of including nanometer-scale talc inclusions (below) resulting in chemical formulae with higher $Si/Si+Fe^{2+}+Mn+Mg$ and $Mg/Mg+Ca+Mn+Fe^{2+}$ ratios than those for Mn-Mg-Fe amphibole

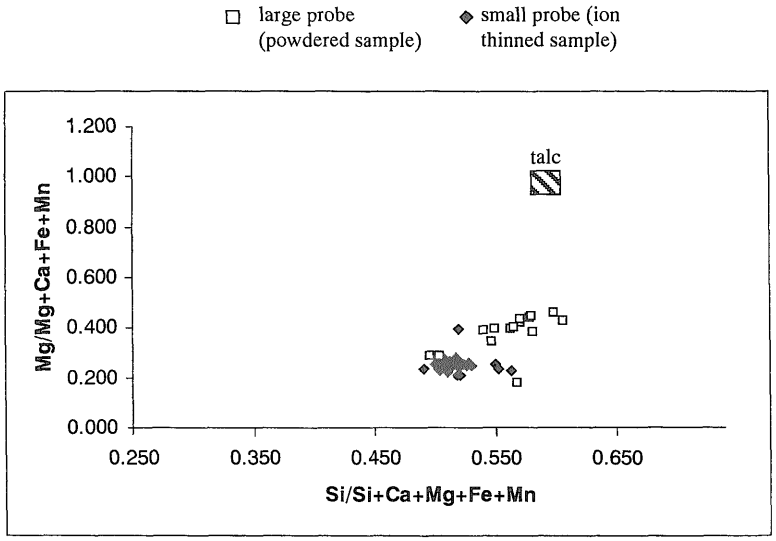

Fig. 9 A comparison of $Mg/Mg+Ca+Fe^{2+}+Mn$ and $Si/Si+Ca+Mg+Fe^{2+}+Mn$ ratios of Mn-Mg-Fe amphibole analyzed with a small beam, ~100–150 nm, and with a large beam, ~800–2000 nm. Note the compositional shift of the latter due to the contribution from nanometer scale talc inclusions (see text for discussion).

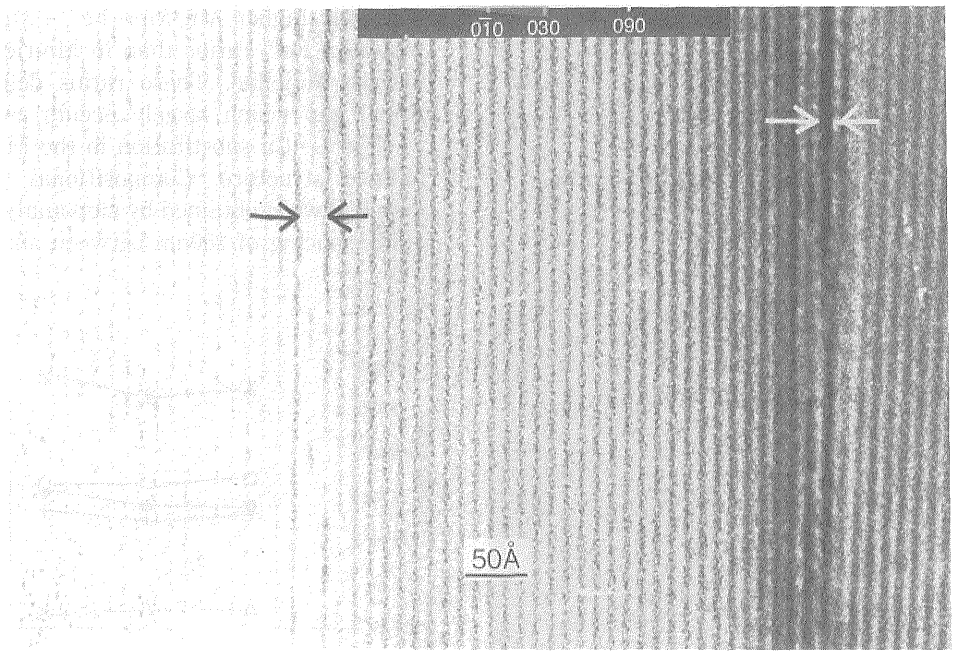

Fig. 10 High resolution transmission electron micrograph showing a triple chain slab, equivalent to the Mn-analogue of clinojimthompsonite, in a regular sequence of double chains. The inset represents the ($0k0$)-zone electron diffraction pattern of the same area. In amphibole, light fringes correspond with slab of double chains (low charge density) and dark fringes with the octahedral slab (high charge density) (see also Fig. 12)

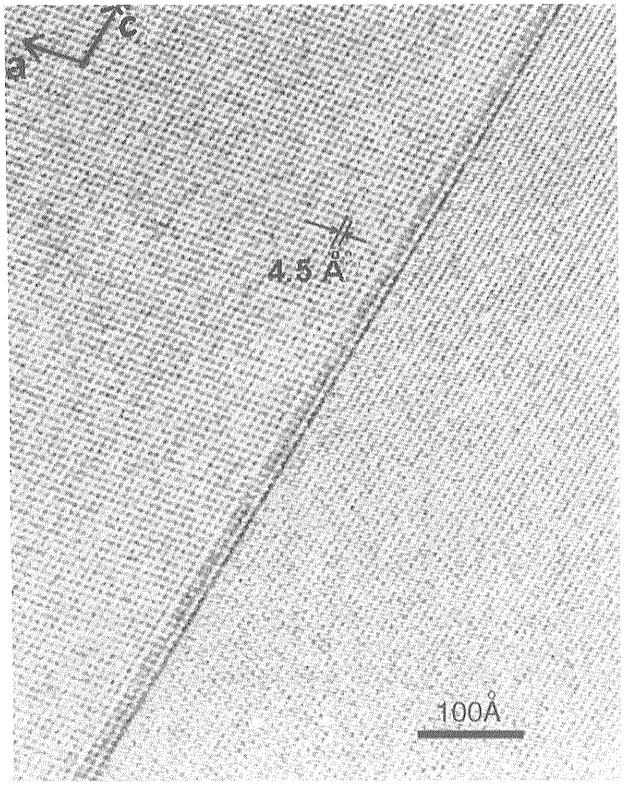

(a)

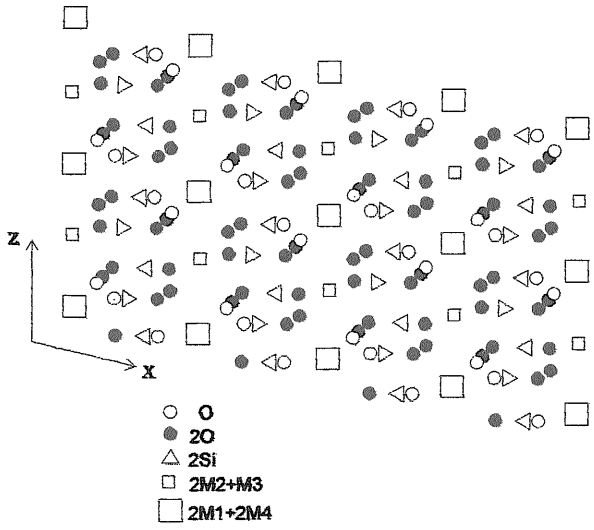

(b)

Fig. 11 a: High resolution image of the (100) twin plane seen edge-on. The section plane is perpendicular to [010]. Note the ~0.15nm thick dark border and the contrast difference between the twin domains, possibly indicating a component of displacement parallel to b (see text for discussions). b: Projection down the y-axis of the amphibole structure (from Hutchison *et al.*, 1975).

obtained using a smaller spot size (Fig. 9). The deviation from the amphibole-talc join is ascribed to submicroscopic quartz inclusions.

5.2 Other fine textures

High resolution TEM images of amphibole were taken at about 150×10^3 magnification and the point-to-point resolution was between 4-5 Å. The HRTEM images (Fig. 10, 11a) are essentially the projection of the charge density of the mineral onto the plane normal to the incident electron beam. At Scherzer focus conditions the light and dark zones respectively correspond to areas of low and high electronic density. Fig. 10 shows the narrow lamellae of triple-chain silicate which occurs as a sporadic fault, less than 1-2 percent. These structures were identified by measuring the spacing of the light fringes which correspond to the chains of Si-tetrahedra (e.g. Akai, 1982). The lamellae, of unit-cell scale width (5-10 nm, at most, in the b-direction), can be considered the manganoan-analogue of clinojimthompsonite (Veblen and Burnham, 1978). As discussed by Thompson (1978), the amphibole double chain structure can be visualized as consisting of alternating pyroxene (P) and mica/talc (M) slabs along the b-direction yielding the sequence .. MPMPMP ... (Fig. 12a). In the case of triple-chain silicate (e.g. clinojimthompsonite), an extra M slab is imposed on the structure and the sequence becomes .. MMPMMPMMP ... (Fig. 12b). The chemical formula of double and triple-chain silicates can be derived by adding up the stoichiometry of the mica (M) slab, $AM_3T_4O_{10}(OH)_2$, and that of the pyroxene (P) slab, $M_4T_4O_{12}$, where A=A-site, M=octahedral site and T=tetrahedral site, in the appropriate proportions. Thus amphibole (MP) is:

$$M_4T_4O_{12}+AM_3T_4O_{10}(OH)_2=AM_7T_8O_{22}(OH)_2$$

and clinojimthompsonite (MMP) is:

$$M_4T_4O_{12}+2AM_3T_4O_{10}(OH)_2=A_2M_{10}T_{12}O_{32}(OH)_4$$

It can be seen that the ratio of tetrahedral cations to tetrahedral and octahedral cations of clinojimthompsonite, 12/22, is higher than amphiboles, 8/15, therefore triple chain faults can increase the Si/(Si+Mtot) ratio in the analysis. In the present case, however, the scarcity of such faults suggests only a limited effect, if any, on the observed shift in composition (see Fig. 9).

Talc platelets have been observed in many Mn-Mg-Fe amphibole grains. They exhibit a topotactic relationship and contact the Mn-Mg-Fe amphibole parallel to (010) planes. The nanometer-scale size of the platelets, smaller than the selected area aperture, precluded determination of the exact orientation relationship. However, Veblen and Buseck, (1981) give $b_{talc}//b_{amp}$ and $a^*_{amp}//c^*_{talc}$, for similar intergrowths. Replacement of Mn-Mg-Fe amphibole by talc at Vittinki is explained by the following retrogressive

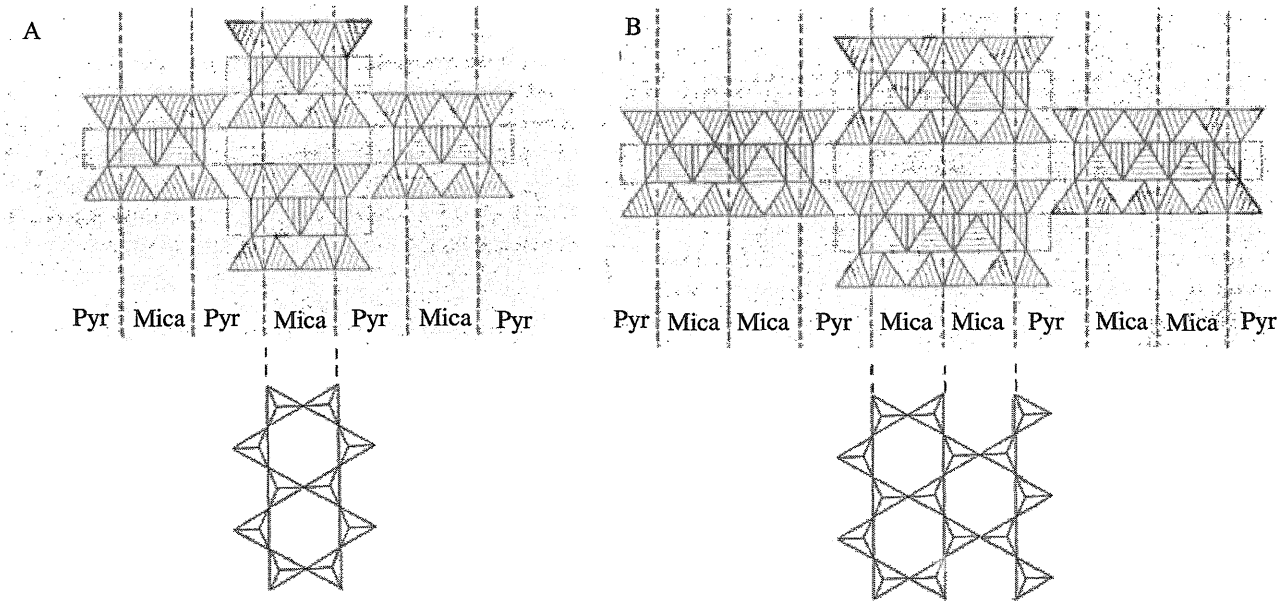

Fig. 12 a: The double-chain clinoamphibole structure consisting of mica(talc) M slabs and pyroxene P slabs alternating in the b-direction, projected along the c-axis (upper) and along the a-axis (lower). b: The triple-chain structure of clinojimthompsonite formed by the same M and P slabs but in the sequence ..MMPMMPMMP ..., viewed as above.

reaction (modified from Akai, 1982):

$$\underset{\text{amphibole}}{(Mn,Mg,Fe,Ca)_7Si_8O_{22}(OH)_2} + Mg^{2+} + 2H^+ \rightarrow \underset{\text{talc}}{2(Mg,Fe,Mn)_3Si_4O_{10}(OH)_2} + Fe^{2+} + Mn^{2+} + Ca^{2+}$$

Micrometer-scale lamellar twinning is present in most of the Mn-Mg-Fe amphiboles examined. The high resolution electron micrograph taken down [010] (Fig. 11a), shows the twin plane as seen edge-on. The 1.5 nm thick dark border is possibly an artifact due to slight misorientation of the section (Horiuchi, pers. com.). Alternatively, it could be a region of intense lattice distortion accommodating the misfit between adjacent twin domains. Elements I and II of the twin show a change of the contrast images. This is the result of a phase shift between the transmitted electron waves (e.g. McLaren, 1991) and is introduced by a lattice displacement vector, R, at the twin boundary with component parallel to the electron beam. The left element of the twin has a pattern of dark spots (about 0.45 nm in size) that, when compared with the amphibole structure (Fig. 11b), possibly correspond to the most electron-dense regions of similar size given by the superposition of 2M1+2M4 (see Hutchison *et al.*, 1975); the right element of the twin has instead a pattern of elongated light spots of low electronic density which possibly correspond to the planes of oxygens.

6. Discussion

6.1 Thermal requilibration

Compared with previously reported examples of Mn-Mg-Fe amphibole coexisting with Mn-pyroxenes and quartz at amphibolite facies (e.g. Peters *et al.*, 1977; Ishida, 1985; Dasgupta *et al.*, 1988), the elevated Ca(M4) (up to 0.44 apfu, Table 3) of some of the analyzed Mn-Mg-Fe amphibole indicates saturation in the actinolite component. The solvus between the Mn-Mg-Fe and Ca amphiboles can be depicted in terms of the exchange of Ca for Mn or Fe in the M4-site with decreasing temperature, and our compositional profile adjacent to the lamellae is consistent with this preposition in that Ca diffuse into the actinolite lamellae whereas Mn and Fe diffuse out from the lamellae. During slow post-peak metamorphic cooling, intervals of undercooling resulted in various stages of coherent exsolution, as indicated by the wide range of lamellar orientation. In ferromagnesian-calcic amphibole pairs, the plane orientations of the "$\bar{1}01$" and "100" lamellae which are optimal phase boundaries (Bollman and Nissen, 1968), are functions of the differences in the lattice parameters Δa, Δc and $\Delta\beta$ of the host and exsolved phases (e.g. Klein *et al.*, 1996). In particular, the "100" lamellar orientation is strongly controlled by the differences in the c lattice parameters, Δc, whereas the "$\bar{1}01$" lamellar orientation is primarily controlled by differences in the monoclinic angle, $\Delta\beta$. Lacking the data on the variation of the lattice parameters with temperature for the Vittinki amphiboles, we cannot estimate quantitatively the exsolution temperatures. However, it is worthy to compare the range of "$\bar{1}01$" lamellar orientations of the studied Mg-Mn-Fe amphibole, 6°, with the "$\bar{1}01$" lamellar orientation of other cummin-

gtonites, 4° (Klein *et al.*, 1996), with exsolution temperatures between 720° and 290°C.

6.2 Mechanism of twinning

The b-component of displacement across the (100) twin plane evidenced by our HRTEM image agrees with the offset along the b-axis in the twinning-assisted transformation from ortho- to clinoamphibole structures (Smelik and Veblen, 1993), which arises from the b/2 component of the n-glide relationship in the (100) plane between the two amphibole lattices. These authors proposed a shearing mechanism similar to that invoked for twinning in pyroxene (e.g. Busek and Ijima, 1974; Smyth, 1974; Coe and Kirby, 1975) (Fig. 13a,b). The mechanism may be construed as a restacking involving half of the octahedral layers; in effect, shearing displaces the oxygen sheets parallel to [001], such that they move from one close-packed configuration to the next. In a perfectly packed octahedral layer, the resulting relative displacements of

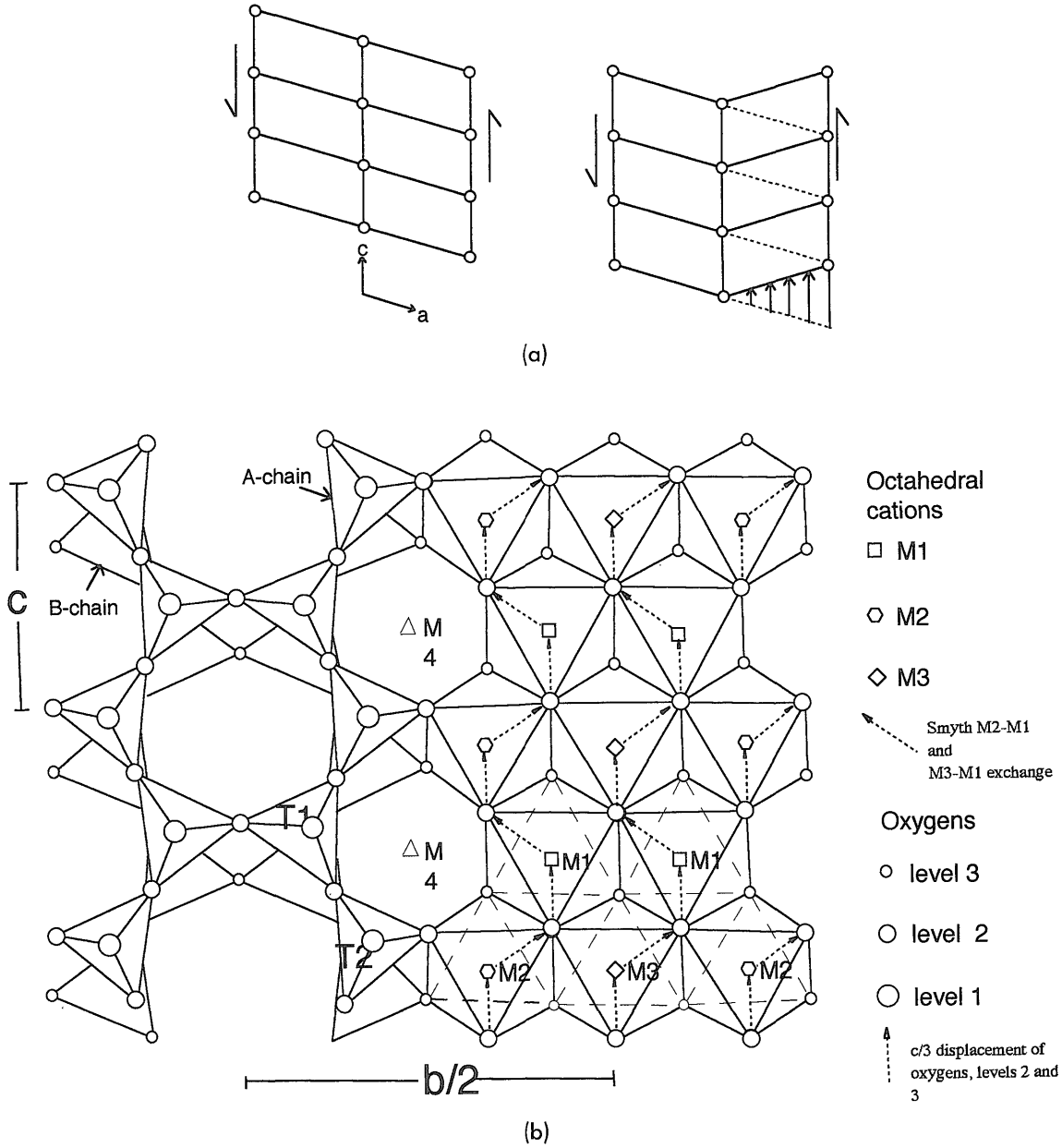

Fig. 13 a: Schematic mechanism of twin by shearing on (100). The sense of shearing is indicated by the arrows. b: Structure of amphibole C2/m projected down a* showing the proposed atomic displacement. The dominant displacement of oxygens can be visualized as a macroscopic shear of octahedral layers by 1/3[001]. The transformation involves movement of the oxygens from one close packed configuration to the next and has component also along b. Note also the movement of the M2- and M3- cations in one octahedral layer to M1 in the next and viceversa, (modified from Coe and Kirby, 1975).

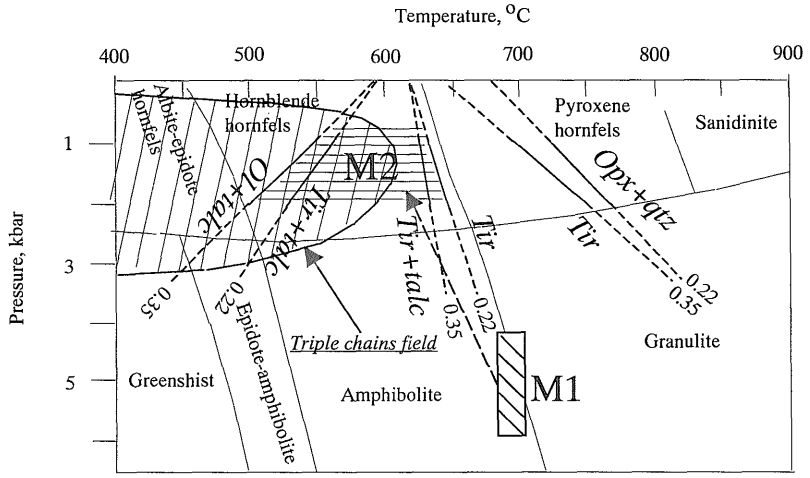

Fig. 14 Estimated metamorphic conditions for the peak (M1) and retrograde (M2) metamorphisms of the quartz-Mn-Mg-Fe amphibole vein at Vittinki, in relation to the stability field of triple chains and disordered pyriboles (adapted from Akai, 1982; Schumaker and Czank, 1987; Akai *et al.*, 1997). The P-T field for the M1 event and the pressure range of 1-2 kbars for the M2 event are based on petrologic and field studies of the regional Svecofennian metamorphism (Korsman, 1988; Kilpeläinen and Rastas, 1992; Kähkönen, 1994; Mancini *et al.*, 1996). The relevant isograds in the Mn-rich system are from Huebner (1986) and were drawn for the minimum and maximum values of the Mn/Mn+Mg ratios in the Mn-Mg-Fe amphibole formulae (Table 1). Mineral abbreviations: Opx=orthopyroxene, Qtz=quartz, Tir=Mn-Mg-Fe amphibole, Talc=talc, Ol=olivine.

the oxygen sheets cause the M2 cations in one octahedral layer to move to M1 in the adjacent octahedral layer (in amphibole, also M3 to M1, Fig. 13b) and vice versa (Smyth, 1974), thus yelding a component of displacement parallel to b.

6.3 Implications for the metamorphism

Triple-chain lamellae are uncommon in the Mn-Mg-Fe amphibole from Vittinki, less than 1-2 percent. The stability relations of triple-chain in nature and in general of disordered pyriboles with quadruple, septuple, etc., chains are unknown but several studies (e.g. Nakajima and Ribbe, 1980; Veblen and Buseck, 1981; Akai, 1982; Schumaker and Czank, 1987) have suggested that they form as intermediate phases of the retrograde conversion of amphibole to talc. In any cases, all the natural occurrences of disordered pyriboles are from rocks that have been metamorphosed at T=250-600°C and moderate pressure, possibly P≤3 kbars (Veblen and Buseck, 1981; Akai, 1982; Schumaker and Czank, 1987; Akai *et al.* 1997), Fig. 14. Recently Akai *et al.* (1997), on the basis of the occurrence of triple chains in supposedly peak-metamorphic orthoamphiboles in ultramafic assemblages, have suggested an upper temperature limit of T=700°C for the formation of disordered pyriboles. However, the matter is controversial because the described post-kynematic amphibole porphyroblasts with triple chains resemble the randomly oriented anthophyllite nematoblasts overgrowing talc-chlorite assemblages in alpine ultramafic rocks and formed at T=600-625°C and P ≤ 4 kbars during alteration at high fCO_2 and low fH_2O (Evans and Tromsdorff, 1974). In addition, the textural relationship of orthoamphibole and intergrown sulfides, which was cited as evidences for the formation of the triple chains at peak metamorphism, might instead be the result of sulfide remobilization and replacement of silicates during retrograde metamorphism (e.g Eckstrand, 1975; Marshall and Mancini, 1994). Thus, the upper limit for triple chain formation is assumed at T_{max}=600°C, Fig. 14, and next we shall discuss the lower temperature limit for retrograde metamorphism of the quartz-Mn-Mg-Fe amphibole veins.

At Vittinki, metasomatic retrogression, involving the gain of Mg and the loss of Ca, Mn and Fe, is implied by topotactic replacement of Mn-Mg-Fe amphibole by talc (above). However, because the talc-isograd is strongly dependent upon XCO_2, it follows that the temperature of talc development will be poorly constrained if the corresponding XCO_2-state is unknown. In the quartz-Mn-Mg-Fe amphibole assemblages at Vittinki, the absence of Mn-bearing carbonates suggests that at peak metamorphism the metamorphic fluids were CO_2-poor (Dasgupta *et al.*, 1988; Gnos *et al.*, 1996). CO_2-poor metamorphic fluids were also present during the replacement of Mn-Mg-Fe amphibole by talc, as no secondary carbonates were formed. This suggestion is compatible with the higher XCO_2 in the adjacent pyroxmangite-rhodonite gneisses (in prep.), since Dasgupta *et al.* (1988) showed that, during metamorphism of Mn-rocks, XCO_2 can vary

from place to place and result in the juxtaposition of carbonate-free (low XCO_2) and carbonate-rich (high XCO_2) facies. A low XCO_2 is also indicated in the quartz-Mn-Mg-Fe amphibole veins by the relatively high Ca-content (up to 0.44 Ca apfu) in some of the Mn-Mg-Fe amphibole, as compared with Mn-Mg-Fe amphibole from similar amphibolite-facies assemblages (e.g. Peters *et al.*, 1977). Therefore, if low XCO_2-conditions are assumed, replacement of the Mn-Mg-Fe amphibole by talc at P=1-2 kbars would have started at temperature of 620-640°C (Huebner, 1986) (Fig. 14), and the paragenesis amphibole+talc constrains the retrogressive M2 metamorphism at T=500-640°C, these conditions being at or slightly above the upper limit for the formation of non-classic pyriboles (Akai, 1982; Schumaker and Czank, 1987; Akai *et al.*, 1997). We finally note that, whereas an elevated XCO_2 favours the formation of disordered pyriboles (Akai *et al.*, 1997), the inferred low XCO_2 during metasomatic retrogression could also have contributed to the scarcity of triple-chain and disordered pyriboles.

Acknowledgments: This study received financial support from the STA-Japan Science and Technology program. We thank Dr. S. Horiuchi (National Institute for Research in Inorganic Materials) for useful comments and discussions. Dr. S. Hagan improved the English of the manuscript.

References

Akai, J. (1982) Polymerization process of biopyriboles in metasomatism of the Akatani ore deposit, Japan. *Contrib. Mineral. Petrol.*, **80**, 117-131.

Akai, J. (1988) Electron microscope observation of "amphiboles" altered from clinopyroxene in the Shimokawa diabases. *Mining Geol. Spec. Issue* **12**, 105-114.

Akai, J., Chiba, A., Konishi, H., Komatsu, M., Matsubara, S. (1997) New occurrences of non classical pyriboles formed during ocean floor metasomatism and regional metamorphism: estimated P-T conditions of formations. *Eur. Jour. Mineral.*, **9**, 1237-1255.

BABEL (Working Group) (1990) Evidence for early Proterozoic plate tectonics from seismic reflection profiles in the Baltic Shield. *Nature* **348**, 34-38.

Bollman, W., Nissen, H. V. (1968) A study of ptimal phase boundaries: the case of exsolved feldspar. *Acta Crystal.* **A24**, 546-557.

Busek, P. R. and Ijima, S. (1974) High resolution electron microscopy of silicates. *Amer. Mineral.* **59**, 1-21.

Champness, P. (1977) Transmission electron microscopy in earth sciences. *Ann. Rev. Earth and Planet. Sci.*, **5**, 203-226.

Cliff, G. and Lorimer, G. W. (1972) Proc. Fifth Europ. Congr. *Electron Microscopy*. Inst. of Physics-London, 140-141.

Cliff, G., and Lorimer, G. W. (1975) The quantitative analysis of thin specimen. *Jour. of Microscopy* **103**, 203-207.

Coe, R. S. and Kirby, S. H. (1975) The orthoenstatite to clinoenstatite transformation by shearing and reversion by annealing: mechanism and potential applications. *Contrib. Mineral. Petrol.* **52**, 29-55.

Dasgupta, S., Bhattacharya, P.K., Chattopadhyay, G., Banaryee, H., Majumdar, N., Fukuoka, M., Supriya R. (1988) Petrology of Mg-Mn amphibole bearing assemblages in manganese silicate rocks of the Sansar Group, India. *Mineral. Mag.* **52**, 105-111.

Eckstrand, O. R. (1975) The Dumont Serpentinite: a model for control of nickeliferous opaque mineral assemblages by alteration reactions in ultramafic rocks. *Econ. Geol.* **70**, 183-201.

Ekdahl, E. (1993) Early Proterozoic Karelian and Svecofennian formations and the Evolution of the Raahe-Ladoga Ore Zone, based on the Pielavesi area, central Finland. *Geol. Surv. of Finland, Bulletin* **373**, 147 p.

Evans, B. W. and Trommsdorff, V. (1974) Stability of enstatite+talc and CO_2-metasomatism of metaperidotite, Val d'Efra, Lepontine Alps. *Amer. Jour. Science* **274**, 274-296.

Gaál, G. (1990) Tectonic styles of early Proterozoic ore deposition in the Fennoscandian shield. *Prec. Res.* **46**, 83-114.

Gaál, G. and Gorbatchev, R. (1987) An outline of the Precambrian evolution of the baltic Shield. *Prec. Res.* **35**, 15-52.

Gnos, E., Armbruster, T., Nyfeler, D., (1996) Kanoite, donpeacorite and Mn-Mg-Fe amphibole: Mn-Mg silicates from a manganiferous quartzite in the United Arab Emirates. *Eur. Jour. Mineral.* 8, 251-261.

Goldstein, J. I., Costley, J. L., Lorimer, G. W., and Reed, S. J. B. (1977) Quantitative X-ray analysis in electron microscope. *SEM 1977*, **1**, 315-325.

Hietanen, A. (1974) Generation of potassium-poor magmas in the Cordilleras and in the Precambrian of Finland. *Geol. Soc. Amer. Abstr.* **6**, 514.

Huebner, J. S. (1986) Nature of phase synthesized along the join $(Mg, Mn)_2Si_2O_6$. *Amer. Mineral.* **71**, 111-122.

Huhma, H. (1986) Sm-Nd, U-Pb and Pb-Pb isotopic evidence foe the origin of the early

Proterozoic Svecokarelian crust in Finland. *Geol. Surv. of Finland Bulletin* **337**, 48 p.

Hutchison, J. L., Irusteta, M. C., Whittaker, E. J. W. (1975) High-resolution electron microscopy and diffraction studies of fibrous amphiboles. *Acta Crystal.* **A31**, 794–801.

Ishida, K. (1985) On the coexistence of Mn-actinolite and Mn-Mg-Fe amphibole from the manganese ore deposits, Japan. *Japan Jour. Min. Soc. Japan* **17**, 1–8.

Kilpeläinen, T. and Rastas, J. (1992) Metamorphism and structures of the nickel-bearing Stormi (Vammala) ultramafic intrusion. *Univ. of Turku, publ.* **30**, 18 p (in Finnish).

Kilpeläinen, T., Korikovsky, S., Korsman, K., & Nironen, M., (1994) Tectono-metamorphic evolution in the Tampere-Vammala area. In: Pajunen, M. (ed.) High temperature-low pressure metamorphism and deep crustal structures. *Meeting of IGCP project 304 'Deep Crustal Processes' in Finland. September* 16-20, 1994. *Geological Survey of Finland, Guide* **36**, 27–34.

Klein, V., Sharp, T. G., Schumacher, J. C. (1997) Analytical electron microscopy of nanometer-scale hornblende lamellae: low temperature exsolution in cummingtonite. *Amer. Mineral.*, **82**, 1079–1090.

Klein, V., Schumacher, J. C., & Czank, M. (1996) Mutual exsolution in hornblende and cummingtonite: composition, lamellar orientation and exsolution temperatures. *Amer. Mineral.* **81**, 928–939.

Kobayashi, H. (1977) Kanoite $(Mn^{2+},Mg)_2Si_2O_6$ a new clinopyroxene in the metamorphic rocks from Tatehira, Oshima Peninsula, Hokkaido Japan. *Jour. Geol. Soc. Japan* **83**, 537–542.

Korsman, K (ed.) (1988) Tectonometamorphic evolution of the Raahe-Ladoga zone. *Geol. Surv. Finland, Bull.* **343**, 96 p.

Korsman, K., Hölttä, P., Hautala, T. and Wasenius, P. (1984) Metamorphism as an indicator of evolution and structure of the crust in eastern Finland. *Geol. Surv. of Finland Bulletin* **328**, 40 p.

Kähkönen, Y., (1994) Shoshonitic and high-K metavolcanic rocks in the southern parts of the Tampere Schist Belt, southern Finland: evidence for an evolved arc-type setting. In: Nironen, M. & Kähkönen, Y. (eds.) Geochemistry of Proterozoic supracrustal rocks in Finland. *Geological Survey of Finland, Special Paper* **19**, 101–115.

Lahtinen, R. (1996) Geochemistry of Palaeoproterozoic supracrustal and plutonic rocks in the Tampere-Hämeenlinna area, southern Finland. *Geol. Surv. of Finland, Bulletin* **389**, 113 p.

Leake, B. E. *et al.* (1997) Nomenclature of amphiboles, report of the Subcommittee on amphiboles of the International Mineralogical Association Commission on new minerals and mineral names. *Eur. Jour. Mineral.* **9**, 623–651.

Mancini, F., Sillanpää R., Marshall, B., Papunen, H. (1996) Magnesian hornblende from a metamorphosed ultramafic body in southwestern Finland: crystal chemistry and petrological implications. *Can. Mineral.* **34**, 835–844.

Maresh, W. V. and Czank, M. (1988) Crystal chemistry, growth kinetics and phase relationships of structurally disordered (Mn,Mg)-amphiboles. *Fortschr. Miner.* **66**, 69–121.

Marshall, B. and Mancini, F. (1994) Major- and minor element mobilization, with implications for Ni-Cu-Fe sulphide remobilization, during retrograde metasomatism at the Vammala mine, southwest Finland. *Chem. Geol.* **116**, 203–227.

McLaren, A. (1991) Transmission electron microscopy of minerals and rocks. Cambridge University Press, 387 p.

Mäkinen, J. (1987) Geochemical characteristics of svecokarelidic mafic-ultramafic intrusions associated with Ni-Cu occurrences in Finland. *Geol. Surv. Finland Bulletin* **342**, 109 p.

Nakajima Y. and Ribbe, P. H. (1980) Alteration of pyroxenes from Hokkaido, Japan, to amphibole, clays and other biopyriboles. *N. Jb. Mineral. Mn.* **1980**, 258–268.

Papunen, H. and Gorbunov, G. J. (Eds.) (1985) Nickel-copper deposits of the Baltic Shield and Scandinavian Caledonides. *Geol. Surv. of Finland, Bulletin* **333**, 394 p.

Peltonen, P. (1995) Petrogenesis of ultramafic rocks in the Vammala Nickel Belt: implication for crustal evolution of the early Proterozoic Svecofennian terrane. *Lithos* **34**, 253–274.

Peters, T. J., Valorelli, J. V., Vcoutinho, J. M. V., Sommeramer, J. & vonRaumer J. (1977) The manganese deposits of Buritirama (Para, Brazil) *Scweiz. Mineral. Petrogr. Mitt.* **57**, 313–327.

Robinson, P., Spear, F. S., Schumacher, J. C., Laird, J., Klein, C., Evans, B. W., Doolan, B. L. (1982) Phase relations of metamorphic amphiboles: natural occurrences and theory. In Veblen D. R. and Ribbe P. H. (eds.) Amphiboles: petrology and experimental phase relations. *Min. Soc. Amer. Rev Mineral.*, **9B**, 1–211.

Ruotoistenmäki, T. (1996) A schematic model of the plate tectonic evolution of Finnish bed-

rock. *Geol. Surv. Finland, Rep. Inv.* **133**, 23 p.
Saxén, M. (1925) Om mangan-järnmalmfyndigheten i Vittinki. Fennia **45**, 1-41.
Schumaker, J. C. and Czank, M. (1987) Mineralogy of triple- and double chain pyriboles from Orijärvi, southwest Finland. *Amer. Mineral.* **72**, 345-352.
Simonen, A. (1980) The Precambrian in Finland. *Geol. Surv. Finland, Bull.* **304**, 58 p.
Smelik, E. A. and Veblen D. R. (1993) A transmission and analytical electron microscope study of exsolution microstructures and mechanisms in the orthoamphibole anthophyllite and gedrite. *Amer. Mineral.*, **78**, 511-532.
Smyth, J. R. (1974) Experimental study of the polymorphism of enstatite. *Amer. Mineral.* **59**, 345-352.
Spry, A. (1969) Metamorphic textures. *Pergamon Press, Oxford*, 352 p.
Thompson, J. B. Jr. (1978) Biopyriboles and polysomatic series. *Amer. Mineral.* **63**, 239-249.
Tuukki, P., (1984) Petrography, mineralogy and geochemistry of quartz-rich metasediments in the Simpsiö and other Pohjanmaa schist districts. *Unpubl. M. Sc. thesis, Univ. of Oulu*, 132 p (in Finnish).
Törnroos, R. (1982) Properties of alabandite: alabandite from Finland. *N. Jb. Miner. Abh.* **144**, 107-123.
Veblen, D. R. and Burnham, C. W. (1978) New biopyriboles from Chester, Vermont: the crystal chemistry of jimthompsonite, clinojimthompsonite, and chesterite, and the amphibole-mica reaction. *Amer. Mineral.*, **63**, 1053-1073.
Veblen, D. R. and Buseck, P. R. (1981) Hydrous pyriboles and sheet silicates in pyroxene and uralites: intergrowth microstructures and reaction mechanisms. *Amer. Mineral.* **66**, 1107-1134.

Received May 25, 1998
Accepted September 7, 1998

西フィンランドのビチンキ累層中のマンガン・マグネシウム・鉄角閃石のナノスケール構造

F. Mancini・丸茂克美・R. Alviola・神山宣彦・B. Marshall

要　旨

西フィンランドのビチンキ累層 (Vittinki Group) 中の高マンガン質片麻岩に伴われる．広域変成作用を受けた石英-マンガン・マグネシウム・鉄角閃石脈の微細構造を高分解能分析電子顕微鏡で観察・分析した．その結果，脈の温度低下に伴われて生成されたと考えられるサブミクロンサイズのマンガン質アクチノ閃石の離溶ラメラが見出された．マンガン質アクチノ閃石の離溶ラメラは($\bar{1}$01)方向と(100)方向のものからなり，(100)ラメラの方向のばらつきは約 11 度，($\bar{1}$01)のそれは約 6 度である．こうしたラメラ方向のばらつきはすでに単斜角閃石で知られており，ラメラ形成が広範な温度域で行われたことを示唆している．($\bar{1}$01)方向のラメラは幅 150-700 ナノメートル，(100)方向のものは幅 70-150 ナノメートルほどであり，こうした幅の相違は元素の拡散速度が均一でないことを示唆している．

高分解能透過電子顕微鏡の像観察の結果，マンガン・マグネシウム・鉄角閃石には，幅 5-10 ナノメートル(b 軸方向)の三重鎖が二重鎖の中にまれに含まれる．一方，マンガン・マグネシウム・鉄角閃から滑石へのトポタキシーは普遍的に認められ，マンガン・マグネシウム・鉄角閃石の化学組成が角閃と滑石との中間であることと調和している．

Appendix 1 Electron microprobe analysis[1] of natural standards, enstatite, phlogopite, and johannsenite[2].

standard	Enstatite (Bumble)	Phlogopite (N. Korea)	Johannsenite
No.	18360	11332	15241
Oxides (wt%)			
SiO_2	57.05(80)	43.04(100)	46.75(9)
TiO_2	0.02(1)	0.42(2)	0.00
Al_2O_3	0.06(2)	16.58(30)	0.48(10)
MgO	33.57(5)	27.10(20)	0.51(300
FeO	9.35(10)	1.36(14)	4.18(20)
MnO	0.07(1)	0.03(1)	27.28(20)
CaO	0.21(5)	0.00	20.37(20)
Na_2O	0.00	0.44(5)	0.00
K_2O	0.01	10.14(80)	0.00
total	100.345	99.13	99.588

[1]Analysis by JEOL at GSJ, using WDS spectrometer at 200sec^{-1} counting time.

[2]Average of 3, 4, 5 analysis respectively.

N.B. the standard deviations (in parenthesis), apply to the last digit.

Appendix 2 Plot of intensity of elements (I_X) versus intensity of silica (I_{Si}) for several standards.